

A Proposal for a Detector 2 km Away From the  
T2K Neutrino Source.

February 16, 2005

## **Proposing Institutions**

*Author list will be here*

## Abstract

We propose building a detector 2km from the neutrino production point of the the T2K experiment.

## Contents

<b>1</b>	<b>Project Description</b>	<b>6</b>
<b>2</b>	<b>Motivation for the 2km Detector</b>	<b>7</b>
<b>3</b>	<b>Overview of the Laboratory Facility</b>	<b>9</b>
<b>4</b>	<b>Water Cherenkov Detector</b>	<b>14</b>
4.1	1kton tank and Substructure . . . . .	14
4.2	Water Purification System . . . . .	15
4.2.1	The primary filling system . . . . .	15
4.2.2	Recirculation . . . . .	15
4.2.3	Temperature control . . . . .	16
4.2.4	Logistics . . . . .	16
4.3	Photomultiplier Tubes . . . . .	16
4.4	Calibration Systems . . . . .	19
<b>5</b>	<b>The liquid Argon detector and its infrastructure</b>	<b>20</b>
5.1	The liquid Argon cryostat . . . . .	23
5.1.1	The dewar and its support structure . . . . .	23
5.1.2	The inner target . . . . .	23
5.1.3	Flanges and services . . . . .	23
5.1.4	Cryogenic infrastructure . . . . .	23
5.2	Liquid Argon process . . . . .	23
5.2.1	Refrigeration . . . . .	23
5.2.2	Liquid Argon purification . . . . .	23
5.3	Liquid Argon monitoring . . . . .	24
5.3.1	Liquid Argon purity monitors . . . . .	24
5.3.2	UV laser calibration . . . . .	24
5.3.3	Slow control . . . . .	24
5.4	Inner detector . . . . .	24
5.4.1	Mechanical structure . . . . .	24
5.4.2	TPC read-out planes . . . . .	24
5.4.3	Wiring procedure . . . . .	24
5.4.4	Electrodes . . . . .	25
5.4.5	Light read-out system . . . . .	25
5.4.6	High voltage systems . . . . .	25
5.4.7	Monitoring and slow control . . . . .	25
5.5	Read-out electronics and trigger . . . . .	25
5.5.1	DAQ system . . . . .	25

5.6	Logistics and installation . . . . .	25
5.6.1	Site infrastructure . . . . .	25
5.6.2	Cryogenics surface and underground equipments . . . . .	25
5.6.3	Safety issues and controls . . . . .	25
5.6.4	Electronics racks and counting rooms . . . . .	25
5.6.5	Installation procedure . . . . .	25
5.7	Detector operation . . . . .	25
5.7.1	Detector commissioning . . . . .	25
5.7.2	Running . . . . .	25
5.7.3	Calibration operations . . . . .	25
5.7.4	Online monitoring . . . . .	25
<b>6</b>	<b>Muon Range Detector</b>	<b>26</b>
6.1	Scintillator detector . . . . .	27
6.2	Electronics, data acquisition and database . . . . .	27
6.3	Muon Range Detector Simulation Results . . . . .	27
6.4	ChD & MRD acceptance and resolution . . . . .	29
<b>7</b>	<b>The 2km Geant4 Simulation and Detector Sensitivities</b>	<b>34</b>
7.1	Water Cherenkov Simulation Result . . . . .	34
7.1.1	Matching SK Resolution . . . . .	36
7.1.2	Muon Momentum Resolution . . . . .	37
7.1.3	Particle Identification Performance . . . . .	39
7.2	Liquid Argon Simulation Results . . . . .	42
7.2.1	Muon Momentum Resolution . . . . .	42
7.2.2	Particle Identification Performance . . . . .	42
7.3	Multi-detector Reconstruction Performance . . . . .	42
<b>8</b>	<b>Physics with the Intermediate Detector</b>	<b>43</b>
8.1	Measurement of the Background for $\nu_e$ Appearance . . . . .	43
8.1.1	Misidentified Charged Current Background . . . . .	45
8.1.2	Intrinsic Beam $\nu_e$ (from Kaons) . . . . .	45
8.1.3	Neutral Current Induced Backgrounds . . . . .	46
8.1.4	Prediction of the Background for $\nu_e$ Appearance at Super-K using the 2km detector. . . . .	46
8.2	Measurement of the Neutrino Spectrum . . . . .	46
8.2.1	near/far ratio . . . . .	46
8.2.2	Measurement of non-QE event rates . . . . .	46
8.2.3	Expected $\theta_{23}$ and $\Delta m_{23}^2$ Sensitivity . . . . .	46
8.3	Physics in the 2nd Phase T2K Experiment with the 2km Detector	46
<b>9</b>	<b>Conclusion</b>	<b>48</b>
<b>A</b>	<b>Schedule</b>	<b>50</b>

<b>B Budget</b>	<b>51</b>
B.1 Water Cherenkov Detector . . . . .	51

# 1 Project Description

*This section is a summary of the document describing motivation and results.*  
(walter)

Rough Overall Document Size Targets:

- Motivation/facilities - 10 pages
- WC Description - 10 pages
- lAr Description - 10 Pages
- Simulation Results + Physics - 20 pages.

## 2 Motivation for the 2km Detector

*The section describes the motivation for the 2km detector complex*  
(walter)

As described in the introduction, T2K is an off-axis experiment. Since the part of the neutrino beam measured by Super-K is only a small portion of the original beam, and it is not the center of the beam, the energy spectrum of the beam seen at Super-K is quite different than the energy spectrum of the entire beam. This is demonstrated by Fig. 1 which compares the neutrino beam spectrum at 280 meters (where the first set of near detectors will be located) with the beam seen by Super-K 295 km away.

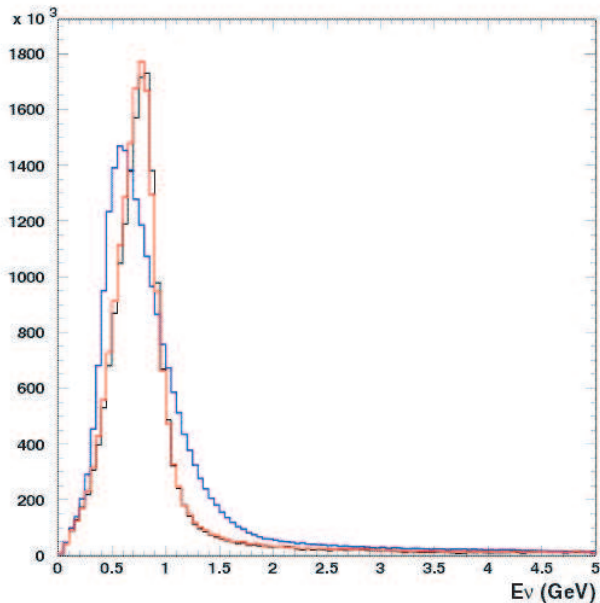


Figure 1: The expected T2K neutrino flux at 280m(blue line), 2km(red line), and SK(black) line.

Measuring the neutrino spectrum before oscillations so as to predict what will be seen at Super-K is important to the search for  $\nu_e$  appearance. The background for the  $\nu_e$  search comes from both electron neutrinos that are intrinsically in the beam at production and misidentified events at Super-K that were produced by  $\nu_\mu$  interactions. Therefore, in order to maximize the potential of the experiment it is important to carefully measure the expected neutrino spectrum for both  $\nu_\mu$  and  $\nu_e$  in a place where the spectrum is as similar to Super-K as possible.

The differences in flux as measured at 280m and 295 kilometers can be seen more clearly by looking at the ratio of near  $\nu_\mu$  flux to far flux (N/F ratio) as a function of energy. The left and right panels of Fig. 2 show this ratio at 280 meters and 295 km respectively. Because the energy of peak positions are shifted at 280m relative to that at Super-K the N/F ratio changes drastically in the region where the oscillation maximum takes place. On the other hand we can see that by moving to around 2km the N/F ratio is flat to about 2%.

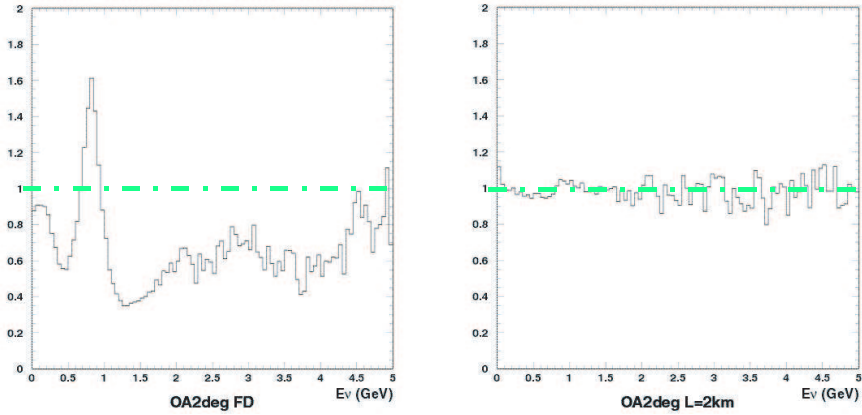


Figure 2: (left) The near/far neutrino flux ratio as a function of energy 280m from the T2K target. (right) The near/far neutrino flux ratio as a function of energy 2km from the T2K target.

There will be a set of detectors built 280 meters from the neutrino source. The profile and properties of the beam near the target will be measured there. Because of the extremely high neutrino flux close to the target, high precision neutrino cross-section measurements will be made. However, the high event rate at 280 meters makes it an unsuitable environment for an unsegmented water Cherenkov detector, due to event overlap.

For this, and the reasons outlined above we propose to build a detector complex 2km away from the neutrino source. The detectors will include a water Cherenkov detector which is the same target material as Super-K in order to cancel neutrino interaction effect, a liquid argon tracking detector and a muon ranger. 2km was chosen as distance by optimizing for the measured event rate and the similarity of the near/far fluxes.

### 3 Overview of the Laboratory Facility

*This section describes the experimental hall and facilities along with detector sizes etc. (Kajita)*

Like K2K we propose to build a detector complex with a water Cherenkov detector, a fine grained detector to measure both the QE and non-QE interactions and a muon ranger. The more finely grained and lower the energy threshold of the detector the better we can do at measuring pions and other particles produced in non-QE interactions and characterizing both the  $\nu_e$  and misidentification to  $\nu_e$  background. For this reason we are proposing to build a liquid argon TPC.

The size of the water Cherenkov detector is driven by two factors. On the one hand we want to contain most muons which interact inside the fiducial volume. At the same time the detector must not be so large that there is more than one neutrino interaction per spill on average. This sets a size of approximately 14 meters with a 9 meter diameter and a 100 ton fiducial volume. The muon ranger must be large enough to contain almost all of the high energy muons produced in the water Cherenkov detector that escape, and must cover enough of the solid angle to intersect most of those muons.

These detector complex must be located on the line that connects between the production target and the far detector. At about 2 km from the target, the center of the detectors must be more than 40 meters below the surface. Therefore, the laboratory facility must be constructed underground as well as the relevant surface facilities. We searched for candidate site for this laboratory facility. We found that there is a candidate site that can house the facility. (However, the candidate site is actually not on the line that connects the target and the Super-K detector. Because of the off-axis beam, the center of the beam is directed to (1.7 to 2.8) degree below and 0.75 degree south of the projected direction to Super-K. This facility is located 1.5 degree south of the Super-K direction. Since the beam is expected to be left-right symmetric, we expect the same flux as that in Super-K. The left-right symmetry of the flux must be monitored by the detector at 280 meters from the target.) Fig. 3 shows the map near J-PARC. The candidate site is located 1.84 km down stream from the target. This place is owned by the local government (Tokai-village). We had many discussions with Tokai-village. In 2003, Tokai-village agreed to rent this place to this experiment without any cost.

Figure 4 shows the details of the site owned by Tokai-village. The layout of the surface and the underground facilities are also shown. In this figure, the surface facility only includes the 2 surface buildings. One building is for the detector monitor and control. We expect one more building for the water purification and liquid Argon production and purification systems.

In order to design the underground facility and to estimate the cost for it, it is necessary to know the condition for the underground soil. For this reason, we have carried out a boring measurement at the site down to 65 meters from the surface in 2003. It turned out that the soil is not heard down to 7.5 meters



Figure 3: A map near the J-PARC accelerator facility and the candidate 2 km detector facility. The horizontal black line near the center shows the line that connect the target and the far detector. The candidate site is shown by a red circle. It is located 1.84 km from the target.

from the surface. However, below this level, the soil is hard enough to excavate the underground facility. The underground facility was designed based on these data.

For cost reasons, the size of the experimental hall must not be larger than absolutely necessary. We have also used this as a constraint in our design studies. Figure 5 shows a completely designed and costed experimental hall. The floor where the neutrino detectors are installed is located 56.27 meters below the surface. The center of the neutrino detectors is 51.62 meters below the surface. The underground cavity is approximately 34.5 meters long, 9.3 meters wide and 14 meters high. This cavity will house the Liquid Argon TPC, the water Cherenkov detector and the muon range detector, from the up-stream to the down-stream. The approximate size of the Liquid Argon detector is 8 meters long and 7 meters in diameter. The size of the water Cherenkov detector is 13.8 meters long and 9.3 meters in diameter. The size of the muon range detector is 7.6m  $\times$  7.6m  $\times$  5m.

The vertical access shaft has 8.5 meters in diameter. There will be one elevator for the access to the underground facility. In addition, there will be one stairway for an emergency exit. Large equipments upto either 4m $\times$ 1m or 3m $\times$ 1.5m can be lowered through this shaft using a crane whose maximum lifting weight is 2.8 tons. At the roof of the underground cavity, there will be another 2.8 ton crane that will run 25 meters along the beam direction.

We will have independent vertical shaft with the diameter of about 1 meter for the ventilation and piping that connect between the surface facility such as

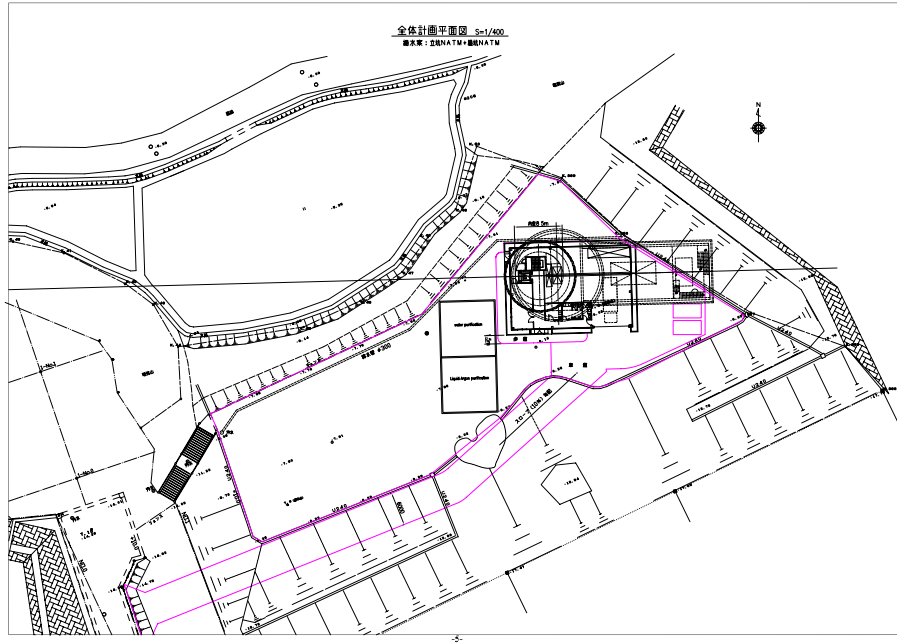


Figure 4: A map near the intermediate detector facility. The area indicated by magenta shows the flat area owned by Tokai-village. The surface buildings are shown by the solid lines. The underground facility is shown by the dotted lines. The access to the facility is from south-west (lower left corner).

the liquid argon production system and the underground detectors.

The surface facility includes 2 surface buildings, one for the operation and monitor of the 2 km detector complex, and the other for the liquid Argon production and water purification systems.

The surface building for the operation and monitor has the dimension of 21 m×14 m. The height should be about 7 m. The building has a control room where physicists take shifts, operating and monitoring the detector complex. In addition, there is a crane whose lifting weight is 2.8 tons. This crane is used to lower heavy equipments to the underground facility.

The water purification system will be mostly located at the surface and a small portion at the first floor below ground (41.77 meters below the surface level) and the bottom of the facility (57.27 meters below the surface level). We plan to generate the pure water from the city water. The main component of the primary pure water system is the Reverse Osmosis system. The other option is to use the primary pure water produced by the pure water system at the J-PARC accelerator facility. In this case, the primary pure water produced at the accelerator facility will be transported to this facility. (Even in this option,

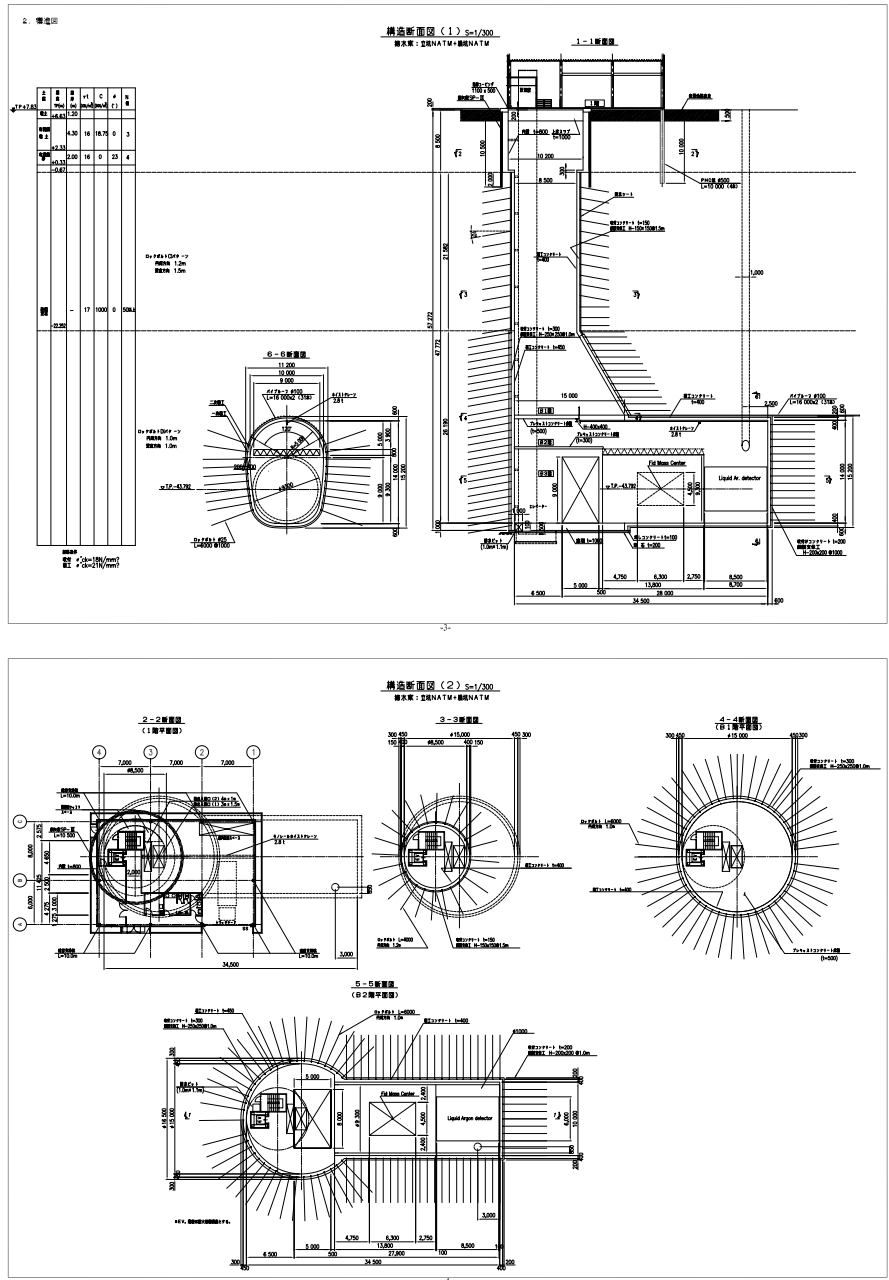


Figure 5: A designed and costed experimental hall. This hall will hold a water Cherenkov detector, fine grained tracker, and muon ranger.

we think we need the primary pure water system for pure water make-up and emergency.) The primary pure water is further purified by the ultra pure water system, which is located on the surface and underground. The ultra pure water thus produced will be fed into the detector tank. The water will be further purified through the circulation between the detector tank and ultra pure water system.

At the surface, there will be a liquid argon production and storage system. The system composed of compressors, storage tanks, ventilation and vaporizers. (However, the argon purification unit will be located underground.)

The second surface building will house the water purification and the liquid argon production systems. The size of the building will be 20 m in length, 10 m in width and 4 m in height.

The total electric power for this facility is designed to be 400 kW. The electricity needed for the water Cherenkov detector including the water purification system, the liquid argon detector, muon range detector and the facility is approximately \*\*\*kW (40kW for the water system), 170kW, \*\*\*kW and 72kW, respectively.

## 4 Water Cherenkov Detector

*This section is a technical description of the WC detector hardware.*

### 4.1 1kton tank and Substructure

The 1 kton water Cherenkov detector will be installed in a water tank of 13.8 meters long. The tank contains cylindrical volume of water of 9.3 meters in diameter and 13.1 meters in length. The tank will be made water tight by plastic lining on the concrete wall for the side wall. The up and down stream of the tank has no concrete wall, and the up and down stream walls must sustain the pressure of the water by themselves. Therefore, the up and down stream walls will be supported by 350 mm H-beams every \*\*\* cm for both vertical and horizontal directions.

Inside the tank, there will be structures to support the photomultiplier tubes. The present design of the structure is shown in Figure 6

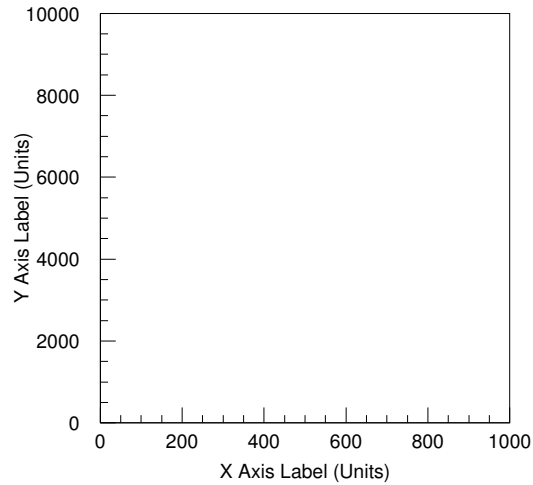


Figure 6: The design of the PMT support structure.

The electronics system will be located at the top of the tank, which is 10.1 meters above the bottom of the tank, The top of the tank is also be used as an underground working space.

The water Cherenkov detector must be calibrated. Therefore, several pipes that allow various calibration equipments from the top of the tank will be prepared.

## 4.2 Water Purification System

We have built several water purification systems for water Cherenkov detectors so the equipment and procedures necessary are well known to us. This detector will be filled with about 1 kiloton of high purity water. Contaminants such as ions, organics, and particulates must be excluded in order to achieve a mean free path for light which is closely matched to the mean free path in Super-Kamiokande (greater than 50 meters in the range of 350 - 450 nm). After filling, this high degree of purity must be maintained in spite of the unavoidable release of contaminants by all materials in contact with the water. In addition, bacterial growth must be minimized.

### 4.2.1 The primary filling system

In principle, reverse osmosis (R.O.), deionization (D.I.) and filtration techniques which are commercially available and actively used, are suitable to achieve water of the quality mentioned above. Deionization provides very good quality water even when the supply water is very poor, but it requires large quantities of caustic chemicals when feed with untreated water. The Reverse Osmosis technique will reject total dissolved solids with an efficiency of about 95%, and will reduce the particulate size to  $\leq 0.001\mu\text{m}$ . R.O., however, requires a large amount of electrical power, and in addition rejects some fraction of the processed water to waste. Therefore in order to conserve power and to minimize waste, we will operate in a mode whereby we fill the detector using the R.O. system and recirculate using the deionizer. The system design is based on our extensive experience in this area from the operation of the IMB, Super-Kamiokande and K2K experiments. Pumps will supply about 20 gallons per minute from a local source to the purification system. Depth filters, carbon filters, a water softener and prefilters will remove silt and particulates to the 10 micron level in preparation for the R.O. membranes. The output of the R.O. unit will go to a degassifier to remove dissolved gasses as a precaution against small bubble formation on the phototube surfaces and to remove radon gas. This will be followed by a sodium exchange anion resin to remove uranium and thorium and then by a mixed bed deionizer. This is followed by more filtration, ultra-violet sterilization and final ultra-filtering before the water is put into the detector. This process will fill the detector in about one week of continuous operation.

### 4.2.2 Recirculation

It is crucial to recirculate the water in the detector through the purification system. This is necessary due to the constant leaching out of substances which reduce the light attenuation length. In addition, the growth of micro-organisms must be inhibited by sterilization during recirculation. The water removed from the detector for repurification will be of high quality-much higher than the quality of the original supply. As a consequence, the recirculation process will be less demanding. Therefore, we can by-pass the pre-treatment stage and the R.O. system and use only the D.I. portion of the original filling system. The

water in the detector will be recirculated in about one week. This procedure will be a cost-effective solution since the chemical costs associated with D.I. of this previously purified water are much lower than the corresponding electrical power costs of the R.O. pumps. Once the detector is filled, therefore, the R.O. system will only be used for additional water that might have to be added to the detector to make up for any losses due to leaks or evaporation.

#### 4.2.3 Temperature control

During recirculation, the water will pass through a chiller unit which will maintain the detector water temperature at 15C. At this temperature bacterial growth will be minimized. The detector tank will be insulated in order to require minimal use of the chiller unit.

#### 4.2.4 Logistics

Some of the components from the water system at the K2K experiment can be reused. These pieces of equipment must be broken down and re-installed at the new location. Our budget includes the labor cost for this procedure.

### 4.3 Photomultiplier Tubes

As we describe in the section on simulation, we have found that the coarse pixelization of 50 cm PMT's in a tank considerably smaller than Super-Kamiokande degrades the pattern-recognition required for efficient  $e/\mu$  identification and ring-finding. This introduces differences in reconstruction efficiencies that become important sources of systematic uncertainty. Our goals for T2K require us to control the systematics extremely well; hence, pixelization becomes an important parameter. Our design incorporates a larger number of smaller diameter PMTs to achieve finer pixelization while 40% photocathode coverage of the detector surface provides the required energy resolution. This arrangement replicates more closely the layout of Super-Kamiokande and will result in better overall performance. Our baseline design therefore uses  $\sim 5350$  eight-inch Hamamatsu R5912MOD PMT's. The Super-K design of waterproof potted base and integrated voltage divider and signal/HV cable will be used; this design has been perfected over the lifetime of the Kamiokande and Super-K detectors. Timely production of these PMT assemblies is no problem; Hamamatsu has, in the past, produced more than 1000 R5912MOD per month. Details of the in-tank mounting structure for the PMT's have yet to be determined. However, with the existing Super-K and K2K (1-KT) detectors as guides, the design and installation should be relatively easily developed.

### Electronics for the Water Cherenkov Detector

The 2km Water Cherenkov detector will require high voltage supplies, DAQ electronics, and ancillary equipment for approximately 7000 PMTs. We propose

to construct the required support electronics and software infrastructure by building upon our extensive experience with the construction, maintenance, and upgrading of Super-K and K2K over the past 10 years, taking into account lessons learned and improvements made or considered.

The electronics and DAQ for 7000 PMTs is well understood by our group and carries no technological, schedule, or cost risks. To be economical, we propose to multiplex high voltage supplies by 12:1, as we do with the Super-Kamiokande outer detector. We have in hand a custom distribution board design, with individually controllable relays to take misbehaving PMTs out of service. Cost of the HV system will be about \$70 per channel.

The analog PMT signal will be sent to custom ADC/TDC boards that are now under development at BU. The new boards will replace the ATM boards[2] presently in use for the SK inner detector. We expect the new boards to have better performance due to new design, better reliability due to decreased number of discrete components, lower power usage due to highly integrated CMOS ASICs, and most importantly much lower cost per channel. We estimate no more than \$200 per channel for front-end electronics. The recorded data will be processed by PC-based workstations. With an event rate of order Hz, there is no particular challenge in accomplishing this.

The one unique requirement of data acquisition for long baseline experiments is the need to accurately and reliably timestamp event records for later matching with the timestamp of accelerator beam spills. This is necessary as running fast signals to the 2km detector, let alone the SK far detector, is prohibitive. For the K2K experiment we have developed a reliable methodology using timestamps generated by duplicate GPS-based systems. At each site, Ru-stabilized oscillators provide a stable local time base that is regularly calibrated and aligned with UTC using GPS data from two independent commercial receivers. In summary, we have specific experience with this aspect of the experiment and foresee no difficulty in meeting requirements.

### **High voltage system**

The PMT high voltage (HV) supply system described here is based on a remotely-controllable rack-mounted “mainframe” manufactured by Universal Voltronics, which acquired the product lines previously supplied by LeCroy. (A system with equivalent features is also available from CAEN, as described below).

One UV-1458 mainframe unit is capable of accomodating sixteen UV-1461 HV modules, providing command and control to each module via user-supplied workstations over ethernet links, or manual operation from its front panel. In turn, each UV-1461 module provides 12 channels of HV, up to 2.5 kV, at 2.5 ma per channel. The mainframe allows each channel to be individually enabled or disabled, and have its voltage set, from the user’s control workstation. It also provides a variety of monitoring and maintenance information upon command.

Each UV-1461 channel has far more current capacity than needed for a single PMT. In order to reduce overall cost, we will multiplex 12 PMTs onto one channel with a custom “paddle card”, to be designed and constructed at

UW. The same method was used in the Super-K Outer Detector (OD), and we can adapt the existing design. Here, we assume that separate HV and signal cables are used for each PMT, as in the Super-K Inner Detector (ID). If, as in the Super-K OD, a single cable is used to carry both the HV supply and PMT output signals, the paddle cards provide a convenient location for picking off signals and isolating the HV. If used, the single-cable arrangement will have negligible effect on the costs estimated here, since the additional parts costs involved are compensated by eliminating the cost of one connector.

Each paddle card distributes the same nominal voltage to the 12 channels it serves, so during pre-construction PMT calibration, we will identify groups of compatible PMTs, i.e. sets of 12 which perform optimally using the same voltage. However, we can make individual final adjustments at the level of a few 10s of volts on the paddle card, using zener diodes. The preliminary design (Figure 7), as in the existing Super-K paddle cards, provides for manual disconnection of individual channels at the front panel (via HV reed relays), indicator LEDs, and on-board connector blocks to allow voltage trimming by relatively easy hand-installation of zener diodes.

To handle 7000 channels, we will need 5 UV-1458 mainframes, and 80 UV-1461 HV modules. These will serve 660 paddle cards to be constructed at UW, by student labor under the direct supervision of a professional engineer (H. Berns). The paddle cards will be housed in 33 crates, each with a low-voltage power supply for the HV cutoff relays. These totals include 10% on-hand spares for swap-in replacements. The total cost for the HV system will be \$500K, as detailed in Table 1 in Appendix B

Since the HV system is directly based on systems previously used at Super-K, with critical components available off-the-shelf from multiple commercial sources, there are no issues of technological, timeline or cost risks involved in its construction. In case Universal Voltronics is unable to supply the equipment required, an almost identical system could be assembled using modules available from CAEN, at essentially the same cost. Thus we have duplicate sources available for the commercially manufactured components.

### **Water Cherenkov Detector Data Acquisition (DAQ) system**

A custom ASIC device is being developed by the BU electronics shop, which has extensive experience in this technology. The highly integrated CMOS ASIC implements in one package the overall system used in the existing Super-K OD front end electronics. A self triggering charge-to-time converter (QTC) provides pulses whose length is proportional to the area under the PMT output signal. Each QTC output is fed to a pipeline time-to-digital converter (TDC), which allows recovery of the full history of a PMT's output over a time window of many microseconds, with nanosecond resolution for edges.

The custom ASICs will be hosted on multichannel DAQ cards, which are in turn housed in VME crates. The crates carry commercial FIFO modules to buffer PMT data, which are then made available on front-end PC Linux-based workstations via DMA interfaces (e.g., Bit3 VME-PCI) or fast ethernet links.

The realtime workstations will apply timestamps obtained from the GPS time synchronization system to each trigger, so event times can be compared between the 2km and far detector sites.

### **GPS time synchronization system**

The K2K experiment demonstrated the successful application of a time synchronization system (??) which used GPS data to provide synchronized UTC time at the near and far detectors. Trigger timestamps provided 20 ns precision and 50 ns absolute accuracy, with great reliability.

We propose to reproduce the K2K system for T2K, taking advantage of eight years of operational experience to introduce minor improvements. The new system will have 10 ns precision, and about 50 ns absolute accuracy. The system maintains time accuracy within these limits as long as it has at least one GPS satellite in range, and its rubidium-stabilized oscillator allows it to maintain time accuracy within 100 ns for periods up to about 5000 seconds if there is a temporary loss of all satellite data (which never actually happened throughout K2K running).

The system will consist of identical installations at each site (JPARC, 2km detector, and Super-K). Each site will be equipped with the following:

- Two independent commercial GPS receivers:
  1. TrueTime rack-mounted XL-DC GPS receiver;
  2. Motorola M12-plus OEM GPS receiver card (mounted on LTC).
- Weatherproof, lightning-protected antennas for each GPS receiver.
- Local Time Clock (LTC) board (custom VME board with rubidium-stabilized oscillator).
- VME crate with power supply.
- VME FIFO module to buffer GPS data.
- VME-PCibus interface, to link PC to VME crate.
- PC workstation (typical 2 GHz, 512 MB RAM, 80 GB disk, ethernet ports, etc) with Linux OS.

In addition, we will supply on-hand spares for each item above, ready for swap-in replacement if needed.

The total cost per site for the equipment listed will be \$80K, including spares. Realtime software, and web-accessible tools for monitoring and control of the system, will be prepared by the UW group under the direction of H. Berns, who designed the corresponding systems for K2K. These costs are summarized in Table 2 in Appendix B.

## **4.4 Calibration Systems**

(Dunmore/Mine/Casper?)

Figure 7: Schematic diagram of the custom HV distribution cards (“paddle cards”).

## 5 The liquid Argon detector and its infrastructure

*This section is a technical description of the LAr Hardware.*  
(Rubbia)

The LAr TPC detector for the T2K 2 km site is hosted in a 8 m long and 7 m diameter stainless steel dewar positioned on mechanical shock absorbers, schematically shown in Fig. 8. Inside the outer dewar an inner vessel of 6 m in length and 6 m in diameter contains the liquid Argon. The volume between the two vessels is evacuated to ensure adequate thermal insulation. The inner vessel contains about 240 ton of liquid. A smaller fiducial volume of about 100 ton is confined by the inner Time Projection Chamber (TPC). The latter consists of a stainless steel mechanical frame with parallelepiped shape inscribed in the inner vessel cylinder.

The cathode of the TPC is placed in the middle of the inner volume, along the longitudinal axis. There are two options for this element, according to the choice we will make about the structure of the inner target, filled with iced water or with solid CO<sub>2</sub>. The first option foresees a cylindrical target structure (Fig. 9) made of a 2 mm thick stainless steel cylinder of 60 cm diameter and 6 m length. In this case, the cathode is a pierced stainless steel plane placed longitudinally along the dewar main axis holding the inner target. The second option refers to a parallelepiped shaped inner target (Fig. 5) 25 cm thick and 6 m long. In this latter case there would be two separate cathode planes placed onto the external sides of the target. In both cases, the cathode electrode defines two half-volumes. Each of the two extreme sides of the half-volumes are equipped with two wire planes with different wire orientation which constitute the readout anodes.

The electric field perpendicular to the wires is established in the LAr volume by means of a high voltage (HV) system in order to permit and guide the drift of the ionization electrons. The system is composed of the above mentioned cathode plane, parallel to the wire planes, placed in the center of the cryostat volume at a distance of 1.8 m from the wires of each side, hence defining the maximum drift path. The HV system includes field shaping electrodes required to guarantee the uniformity of the field along the drift direction, and a HV

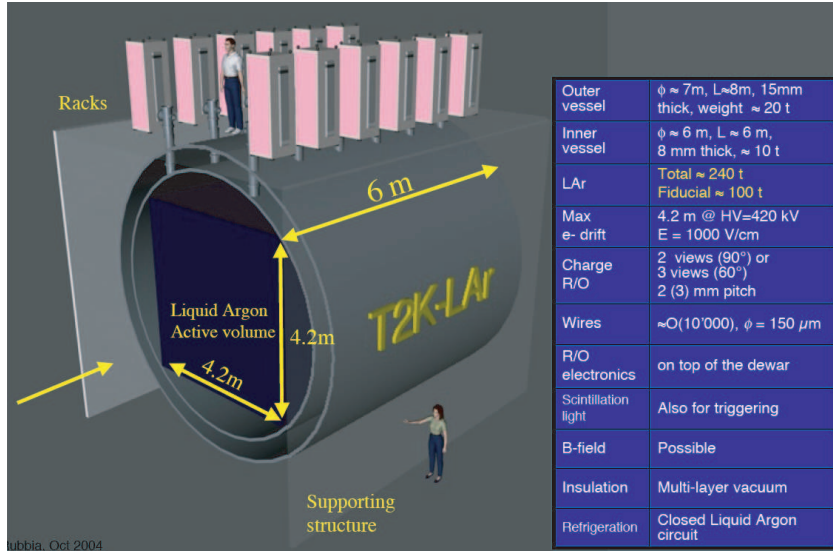


Figure 8: Artistic view of the proposed 100 ton liquid Argon TPC detector.

feedthrough to set the required potential on the cathode. At the nominal voltage of xx kV, corresponding to an electric field of xxx V/cm, the maximum drift time in LAr is about 1 ms.

Large surface photomultipliers (PMTs) are placed inside the liquid, attached to the supporting mechanical structure, outside the inner fiducial volume.

On top of the cryostat there are flanges equipped with cryogenic feedthroughs for the electrical connection of the wires with the read-out electronics, and for the internal instrumentation including PMTs, purity monitors, level meters, temperature probes, etc. The electronics allow for continuous read-out, digitization and wave-form recording of the signals from each wire of the TPC. The front-end electronics is host in 12 crates directly placed on top of the dewar.

The passage of charged particles inside the LAr volume produces both ionization and scintillation light signals. Detection of this light by the PMTs provides a method for the absolute time measurement of the event and an internal trigger signal. Reconstruction of ionizing tracks is performed by using charge and the light signals. Ionization electrons induce detectable signals on the TPC wires during their drift towards and across the wire planes while and UV photons from scintillation provide a prompt signal on the PMTs that allows the measurement of the absolute drift time and, hence, of the distance traveled by the drifting electrons. In this way, each of the planes of the TPC provides a two-dimensional projection of the event image, with one coordinate given by the wire position and the other by the drift distance. A 3D reconstruction of the event is obtained by combining the information from wire planes occurring at the same drift distance.

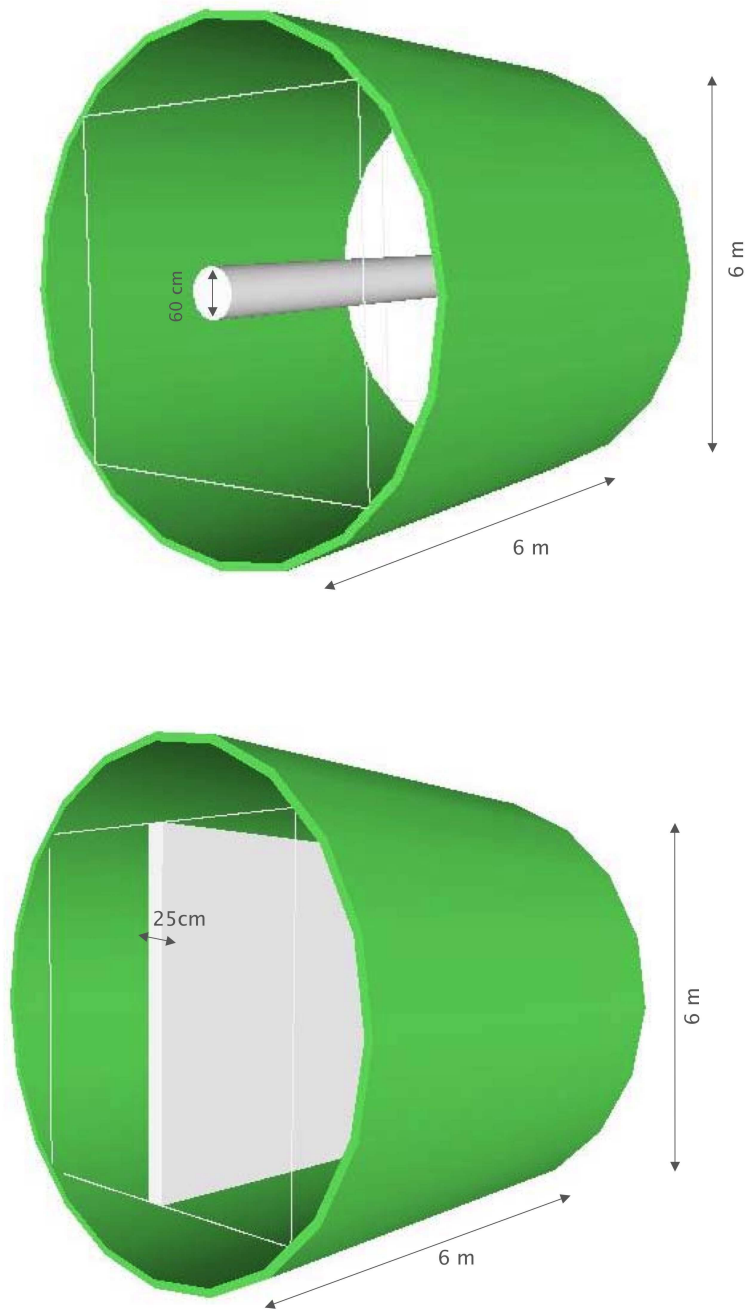


Figure 10: The option of a parallelepiped shaped inner target .

Some of the PMTs may also be optimized for the detection of Cerenkov light produced in LAr, a process that has been studied by the ICARUS Collaboration [1]. This feature may provide additional handles to improve the quality of the event reconstruction.

We finally observe that the events occurring in the inner water (CO<sub>2</sub>) target are reconstructed by the detection of particle tracks escaping from the target into the external (instrumented) liquid Argon TPC volume.

The detector is complemented by ancillary cryogenics systems. A gas and liquid recirculation and purification system, a heat exchanger and a LAr buffer are placed in the underground cavern, close to the detector dewar. These equipments are connected through cryogenic pipes to surface, where Argon storage, compressor, ventilation and evaporation systems complete the detector infrastructure.

## **5.1 The liquid Argon cryostat**

### **5.1.1 The dewar and its support structure**

#### **5.1.2 The inner target**

The main motivation of the inner target is to collect a sample of neutrino interactions with Oxygen nuclei, analogous to those occurring in the far Super-Kamiokande detector, but with the particle tracks entering the liquid Argon imaging volume. One could therefore reconstruct in detail these events by exploiting the low threshold of the TPC detector and its ability in reconstructing multi prong events.....

The inner target geometry has been studied by means of simulations.....

#### **5.1.3 Flanges and services**

#### **5.1.4 Cryogenic infrastructure**

## **5.2 Liquid Argon process**

### **5.2.1 Refrigeration**

#### **5.2.2 Liquid Argon purification**

For a correct operation of the detector and in order to reach a sufficiently high value for the drifting electron lifetime, liquid Argon has to be pure with a concentration of electronegative impurities lower than 0.1 part per 10<sup>9</sup> (ppb) O<sub>2</sub> equivalent during all phases of the detector operation. This can be achieved by using suitable materials, cleaning, and careful design of the internal components, as well as vacuum conditioning of the internal surfaces, since pollution of the LAr is mainly due to outgassing of the inner surfaces in contact with the gaseous Argon. Standard Oxysorb/Hydrosorb filters<sup>1</sup> provide a purity level which is well above the experimental requirements.

---

<sup>1</sup>Hydrosorb and Oxysorb are registered trademarks of Messers-Greisheim.

Injection of Argon from the external storage is performed through xxx sets of Oxysorb-Hydrosorb filters placed in series. Each unit is made of four identical cartridges in parallel and filled for 1/3 with Hydrosorb and for 2/3 with Oxysorb. Each set of filters is dimensioned to allow for the purification of the LAr volume starting from standard commercial LAr (with a concentration of H<sub>2</sub>O and O<sub>2</sub> of about 0.5 ppm). The nominal purification speed is xx LAr m<sup>3</sup>/hour. The presence of xx cartridges in series provides a safety margin in case of unexpected contamination of the industrial LAr.....

### **5.3 Liquid Argon monitoring**

#### **5.3.1 Liquid Argon purity monitors**

#### **5.3.2 UV laser calibration**

#### **5.3.3 Slow control**

### **5.4 Inner detector**

The inner detector is composed of a rigid mechanical frame made of .....

#### **5.4.1 Mechanical structure**

#### **5.4.2 TPC read-out planes**

In the baseline detector design one has two TPCs (Left and Right chamber) placed inside the cryostat placed along the beam direction. Each TPC consists of a system of two parallel wire planes 3 mm apart from each other. The distance between the two TPCs is about xx m, with the cathode plane, parallel to the wire planes, placed in the middle. This sets at xx m the maximum drift length of the active volume for both chambers.

Wire directions in the planes run at  $\pm 45^\circ$  with respect to the horizontal direction. The planes closer (farther) to the cathode are called Induction-1 (Induction-2) planes. The wire pitch can be 2 or 3 mm according to the the different detector options.....

#### **5.4.3 Wiring procedure**

As already mentioned, wires are made of stainless steel with a diameter of 150  $\mu\text{m}$ .....

- 5.4.4 Electrodes
- 5.4.5 Light read-out system
- 5.4.6 High voltage systems
- 5.4.7 Monitoring and slow control
- 5.5 Read-out electronics and trigger
  - 5.5.1 DAQ system
- 5.6 Logistics and installation
  - 5.6.1 Site infrastructure
  - 5.6.2 Cryogenics surface and underground equipments
  - 5.6.3 Safety issues and controls
  - 5.6.4 Electronics racks and counting rooms
  - 5.6.5 Installation procedure
- 5.7 Detector operation
  - 5.7.1 Detector commissioning
  - 5.7.2 Running
  - 5.7.3 Calibration operations
  - 5.7.4 Online monitoring

## 6 Muon Range Detector

*This section is a technical description of the MRD detector hardware.*

In order to increase the accuracy of the determination of the incident neutrino beam at high energy the WC and lAr detector can be completed with a Muon Range Detector (MRD). The Main requirements for the muon range detector are as the following:

- (1) The detector has to measure muon energy in the range of the expected neutrino spectra with reasonable resolution,
- (2) Due to limited space in the underground hole, the length of MRD can not be more than 5m.

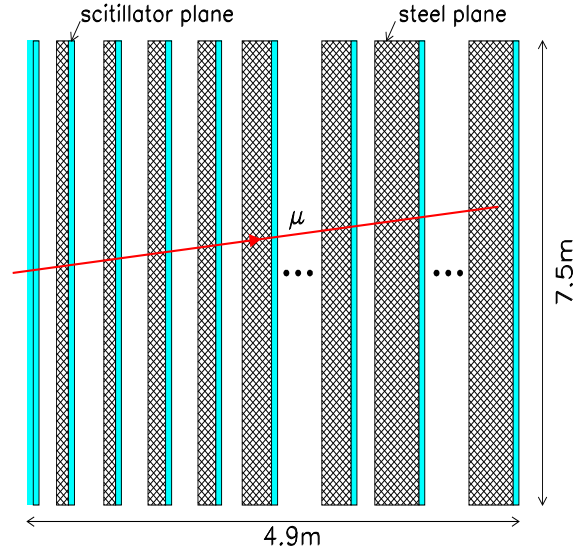


Figure 1: Setup of the Muon Range Detector .

The MRD consists of 22 steel planes each followed by a scintillator plane. In addition, two additional scintillator planes are 9 cm before the first steel plane. This setup is shown in Fig.1. The size of the MRD is 7.5 m × 7.5 m × 4.9 m. In order to have good energy resolution for the entire energy region, the first two upstream steel plates are 2.5 cm thick, the next two planes have thickness of 5 cm, the next ten layers are of 10 cm thick, and the downstream eight are 20 cm. A setup with the upstream four steel planes having 5 cm thickness was also considered. A center-to-center spacing between upstream fourteen steel planes is 19.1 cm, with 29.1 cm between the downstream eight planes.

Figure 2: FIGURE CAUSES PROBLEMS. COMMENTED OUT. Sketch of the scintillator planes and plastic strip.

Each scintillator plane is made up of 187 strips, each one of 4 cm wide, 1cm thick, and 7.5 m long. The orientation of the strips alternates by  $\pm 90^\circ$  in successive planes (X and Y modules) as shown in Fig.2. Each scintillator strip has a wavelength shifting fiber embedded in it to capture, wavelength shift, and transport the light to the two ends. Both ends of each fiber are couplet through clear fibers and multiplexing boxes to multiplex photomultiplier tubes. The total MRD thickness (including scintillator) of  $2185 \text{ g/cm}^2$  corresponds to muon energy of  $\approx 3.5 \text{ GeV}$ .

### 6.1 Scintillator detector

### 6.2 Electronics, data acquisition and database

### 6.3 Muon Range Detector Simulation Results

Charged-current neutrino events have been simulated in fiducial volume of ChD using the calculated neutrino energy spectrum at distance of 2km from neutrino production point for the off-axis beam. The peak neutrino energy is tuned to the oscillation maximum of  $\sim 0.8 \text{ GeV}$  and spectrum continues up to  $\sim 15 \text{ GeV}$ . The spectrum of muons that penetrate into MRD through the vertical wall of the Cherenkov detector (Fig.5) have been used for simulation of the MRD response.

Three-dimensional MC codes for simulation of muon transport through ChD and MRD have been applied. The codes allow either to consider the average ionization energy loss calculation along tracking step, or to account for fluctuations either by explicit  $\delta$ -ray production above a given energy out (in this simulation the  $\delta$ -electrons energy cut of 1 MeV is used) or by a computed fluctuation function (Gaussian or approximating the Landau shape). Muon transport is performed with variable optimized steps. The program performs also the discrete sampling of bremsstrahlung, inelastic muon-nuclear interaction and pair production processes.

A special feature of this program is the 3-dimensional simulation of the muon tracks. The recent treatment of multiple Coulomb scattering of muons is used [1]. In this approach the muon angular distribution is similar to Moliere distribution after passing through the small thickness of material and moderate deflection angles. However, at large thickness of scatterer, the angular distribution is drastically changed by influence of the nuclear form factor. Multiple scattering and lateral displacement are regarded as continue process occurring along muon track.

The algorithm for muon track and energy reconstruction is based on the least square method and described in [2],[3],[4]. It takes into account contributions of the position measurement error, energy loss and Coulomb scattering.

The result of a muon energy reconstruction by the MRD, i.e. the scattered plot of truth muon energy at the entry into MRD  $E_0$  versus reconstructed energy  $E_{rec}$  is presented in Fig.3. The obtained relationship between  $E_0$  and  $E_{rec}$  to be related to the discrete structure of the range detector. The muon energy range which can be measured by the MRD is  $0.125 \div 3.5$  GeV.

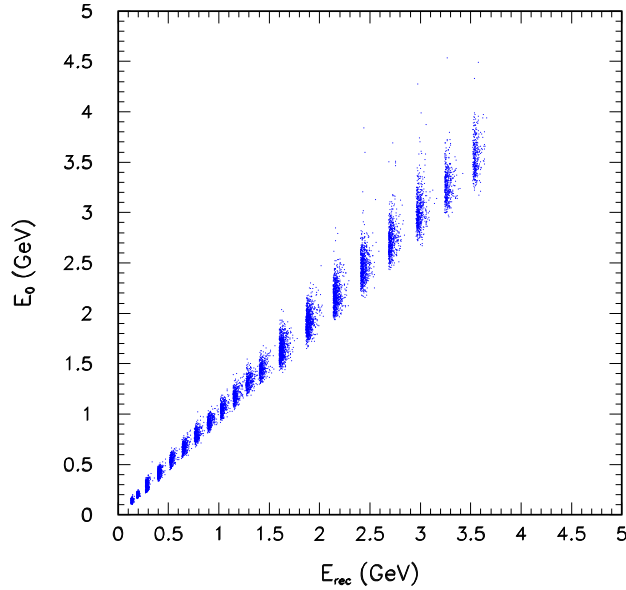


Figure 3: Muon energy  $E_0$  at the entry into the MRD vs. reconstructed energy  $E_{rec}$ .

Figure 4 (top panel) shows the dependence of the mean value of  $\langle \Delta E/E \rangle$  (which is taken as energy resolution) on the muon energy, where  $\Delta E = E_0 - E_{rec}$ . The differences in the truth and reconstructed muon directions  $\Delta\theta$  (angular resolution) is plotted in Fig.4 (bottom panel) also. The vertical bars show the  $\sigma(\Delta E/E)$  and  $\sigma(\Delta\theta)$ , correspondingly. The energy resolution is of  $\sim 1\%$  and  $\sigma(\Delta E/E) = 5 \div 7\%$  at  $E \leq 3.5$  GeV;  $\Delta\theta$  decreases with muon energy from  $\sim 6^\circ$  up to  $1^\circ$

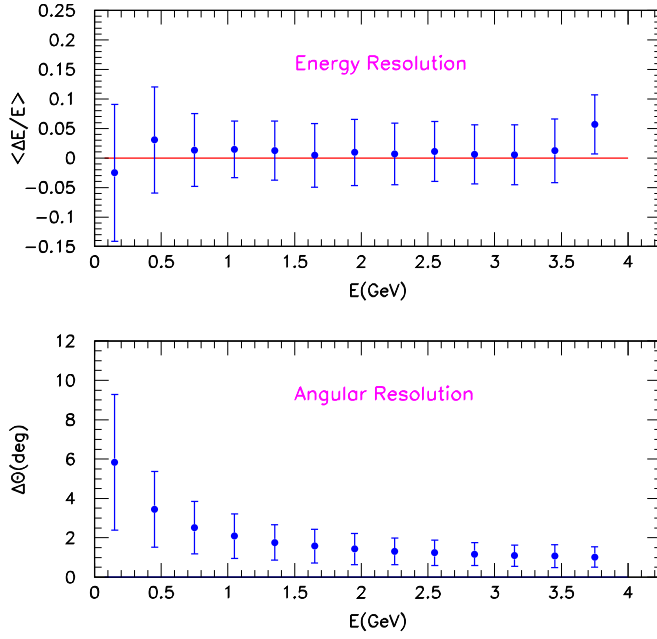


Figure 4: Energy (top panel) and angular (bottom panel) resolutions of the MRD vs. muon energy. The vertical bars show the  $\sigma(\Delta E/E)$  and  $\sigma(\Delta\theta)$ .

## 6.4 ChD & MRD acceptance and resolution

To estimate the efficiency of operation two detectors in coincidence we regarded case when water Cherenkov detector (size, layout and PMTs as in the case of the 1kt tank at K2K) is completed by the muon ranger at the distance 74 cm. The schematic view of ChD&MRD is shown in Fig.5 (top panel)

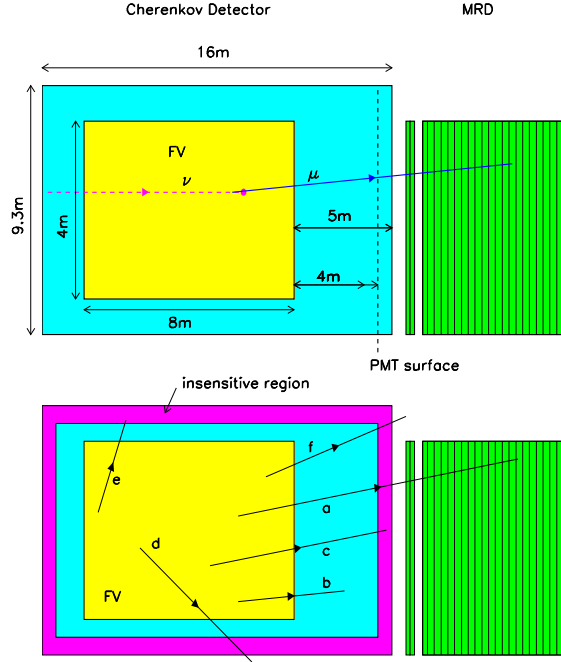


Figure 5: Sketch of the layout of water Cherenkov detector and muon ranger (top panel). Event types produced by neutrino in fiducial volume (bottom panel).

The ChD is the cylindrical tank of 9.3m diameter and 16m length. The size of fiducial volume (FV) is 4m in diameter and 8m in length. The distance between FV and PMT surface in forward direction is 4m. The thickness of insensitive region is  $\approx 1.5$ m. Neutrino events produced by CC neutrino interaction in the fiducial volume have been simulated and reconstructed (vertex position, muon momentum etc) using the code and methods developed for the 1kt detector. Different types of muon events are shown in Fig.5 (bottom panel).

The types of events are as follows

- a) stopping muons in the active MRD region
- b) stopping muons in the sensitive ChD region
- c) stopping muons between the active water region and the active MRD region
- d) penetrating muons through the barrel wall
- e) stopping muons in the barrel side insensitive region
- f) penetrating muon through the vertical wall of the ChD

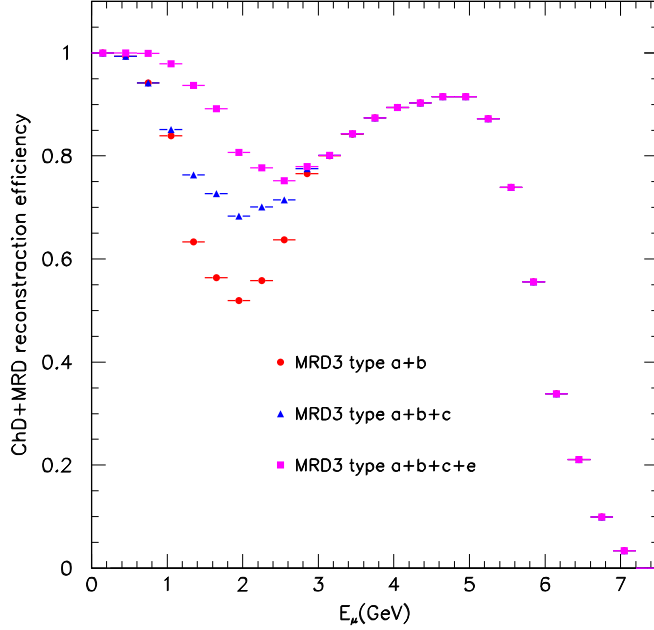


Figure 6: ChD&MRD reconstruction efficiency as a function of muon energy.

The detection efficiencies of the different events as a function of the muon energy are shown in Fig.6. For the events of the a+b) type it has minimum of  $\sim 52\%$  in the energy bin  $1.8 \div 2.1$  GeV. The events of the c) type may be detected, using the scintillator plane between the active water region of the ChD and the active region of the MRD, like outer detector. The events of the e) type, in principle, may be detected also by a barrel-side outer detector. But the energy resolution of such kind events will be worse in comparison with events of the a) and b) types. The efficiencies for events of the a+b+c) and a+b+c+e) types are shown in Fig.6 also. In the last case the minimal efficiency is equal of  $75\%$  in the energy bin  $2.4 \div 2.7$  GeV.

The muon energy reconstruction method for events of the a) type is described in [4].

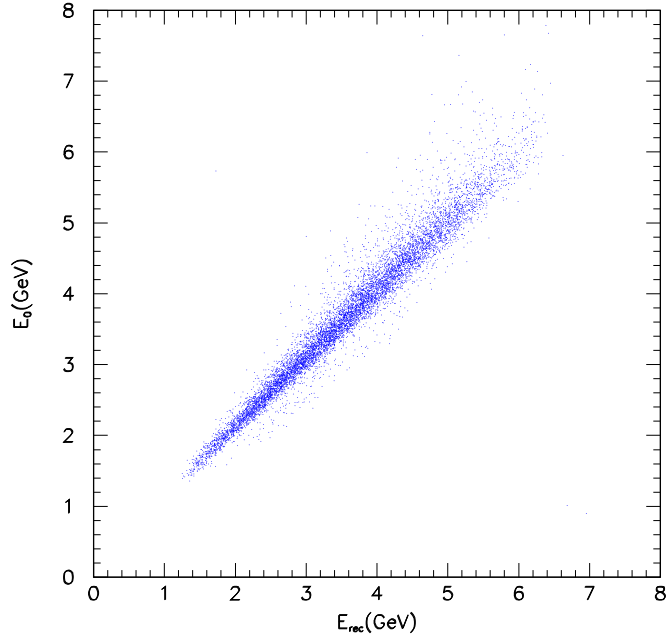


Figure 7: Muon energy at the production  $E_0$  as a function of reconstructed energy  $E_{rec}$ .

Multi-detector reconstruction performance are presented in Figs.7,8. The scattered plot of  $(E_{rec}, E_0)$ , is shown in Fig.7, where  $E_{rec}$  is the reconstructed muon energy and  $E_0$  is the generated one. The energy  $\langle \Delta E/E \rangle$  and angular  $\Delta\theta$  resolutions of the ChD&MRD is given on Fig.8 as functions of the muon energy, where the vertical bars show the  $\sigma(\Delta E/E)$  and  $\sigma(\Delta\theta)$ . The energy resolution  $\sigma(\Delta E/E)$  equals to 5% – 6% and don't depend on muon energy in region 1.2÷6 GeV. The angular resolution  $\Delta\theta$  decreases with energy from  $\sim 3^\circ$  upto  $\sim 0.7^\circ$ .

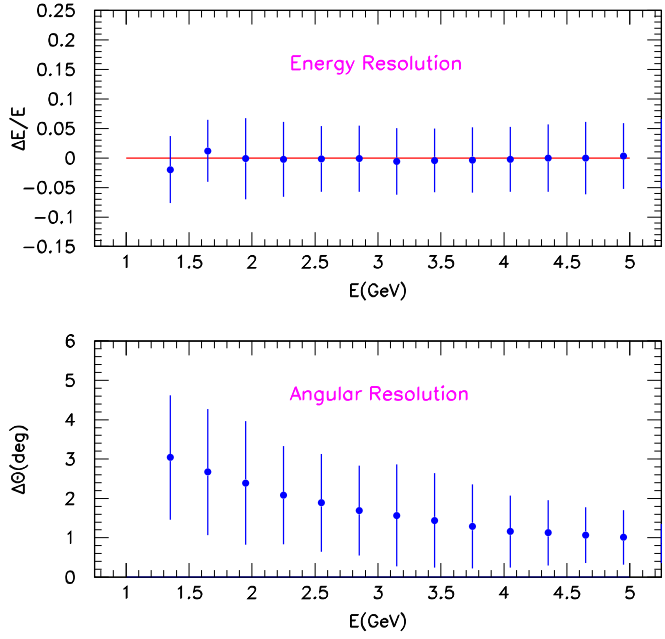


Figure 8: Energy (upper) and angular (lower) resolutions of the ChD&MRD vs. muon energy. The vertical bars show the  $\sigma(\Delta E/E)$  and  $\sigma(\Delta\theta)$ .

## 7 The 2km Geant4 Simulation and Detector Sensitivities

*This section describes the G4 simulation framework and the results of the simulation. This describes the tracking, PID performance etc. Although the ability to distinguish  $\nu_e$  is covered here, the application to the T2K neutrino beam is covered in section 8*

(Scholberg/Fechner/Rubia)

In order to design the 2km detector complex, a complete GEANT4 simulation program was written. GEANT4 was chosen since it is now used by many HEP collaborations, and is well supported. The simulation reads input neutrino and particle vector files. The simulation outputs ROOT files which can then be processed by ROOT or, in the case of the WC detector, converted and processed by the standard SK reconstruction software.

### 7.1 Water Cherenkov Simulation Result

Much work has gone into making the water Cherenkov part of the code as flexible as possible. We can adjust both detector size and layout including the size of the PMTs, allowing us to simulate any water Cherenkov detector, and to compare against the 1kt tank at K2K, for which we already have a large data set of beam neutrinos. We are presently using this to validate the GEANT4 MC by:

- Simulating the 1kton tank at K2K
- Comparing the output between the GEANT4 and the K2K MC
- Tuning various parameters such as water scattering to get reasonable agreement
- Comparing the GEANT4 output against K2K neutrino interaction and cosmic ray data

In order to do this we have generalized the SK/K2K reconstruction code and converted the Root output from our MC into a format readable by the Super-Kamiokande tools. We were then able to run the full Super-Kamiokande reconstruction suite on the output of the MC.

We first compared the MC performance by comparing with vertical through-going muon data. Vertical through-going muons are minimum ionizing particles and produce a clear Cherenkov cone ; they are a well known calibration source at SK and the K2K 1kton detector. We used the same input for the GEANT4 MC as is used at K2K for simulating through-going muons, and the same through-going muon fitter. An example of this is shown in Figure 11, where the total charge collected at all of the PMTs in the tank is shown for the GEANT4 MC and actual data. This first stage allows us to tune the charge scale (amount of

Cherenkov light emitted by a minimum-ionizing particle per unit track length) and measure the amount of indirect light (scattered and reflected light outside the Cherenkov cone). The results are shown in Figure 12. After this initial tuning, the charge scale difference between data and MC is  $1.8\% \pm 0.2\%$ .

For the second stage of the tuning we simulated K2K beam  $\nu_\mu$  events, using the same neutrino flux and neutrino interaction simulation as the K2K 1kton group. These events were processed using the full 1kton reconstruction suite. In order to check the energy scale, neutrino-induced  $\pi^0$  events are selected : a single  $\pi^0$  enriched event sample is obtained by selecting 2 *ring e-like* events (i.e. events where two tracks are found and identified as electromagnetic showers). The invariant mass distribution for those events is computed, and a  $\pi^0$  mass peak is obtained, shown in Figure 13. The relative difference between the data and GEANT4 MC peak is  $-6.0\% \pm 0.7\%$ . The peak for both the data and MC are shifted slightly higher than the true  $\pi^0$  mass, which can be accounted for by vertex reconstruction biases and extra energy deposited by  $\gamma$ 's from oxygen nuclei. The differences between data and MC for through-going muons and neutrino events are mostly caused by a slight excess of indirect light in the MC, which affects the Cherenkov ring patterns and energy determination. They can be corrected by adjusting the reconstruction software<sup>2</sup>. These results confirm that the GEANT4 simulator is suitable for studying other detector geometries.

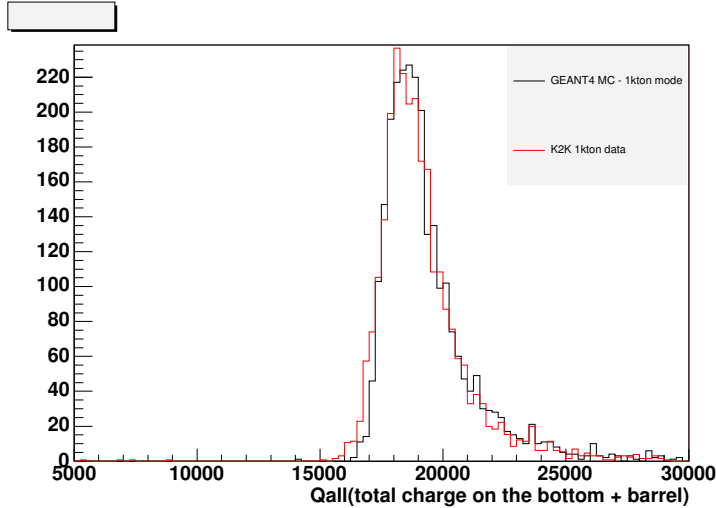


Figure 11: Comparison of collected charge from the PMTs in events between a the GEANT4 simulation configured with the geometry of the K2K water Cherenkov tank and real downward going muon data.

As can be seen, after our initial tuning, there is quite good agreement.

<sup>2</sup>This is not done for the comparison with K2K data, in order to check the performance of the simulator itself.

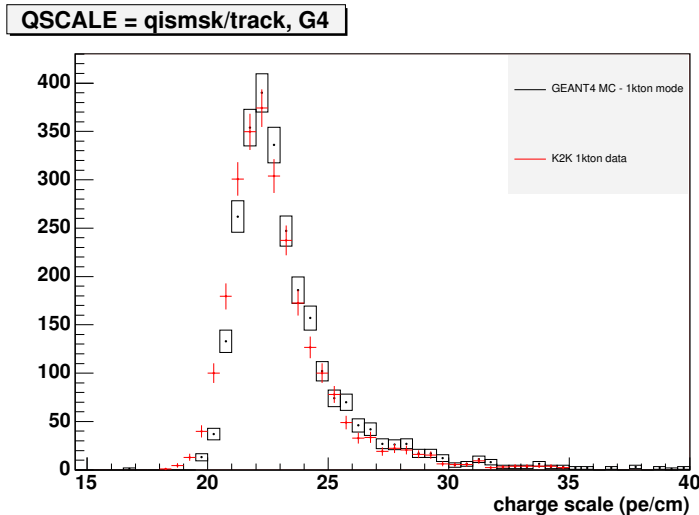


Figure 12: Comparison of the charge-scale distribution (ratio of the total collected charge and the reconstructed track length) between the GEANT4 simulation configured with the geometry of the K2K water Cherenkov tank and real downward going muon data.

### 7.1.1 Matching SK Resolution

The philosophy behind the design of the K2K water Cherenkov detector was to use exactly the same hardware and electronics as in Super-Kamiokande so as to cancel out as many systematic errors between the two detectors as possible. For T2K we are designing the detector to match the response of the near detector at 2km with Super-Kamiokande, even if it means using a different hardware configuration. This means choosing a configuration which has the most similar response when reconstructing physics quantities. This work is just beginning. An example is the choice of the size and number of PMTs. One option is to use the same size PMTs as K2K and Super-Kamiokande. However, the number of PMTs, and hence the ring resolution is greatly reduced due to the relatively large “pixel” size. Another option is to use a larger number of 8-inch PMTs. Although the physical size of the PMT is different, the number (6160 vs. 841) is much closer to Super-Kamiokande and the relative pixel sizes are similar. Figure 14 demonstrates this effect. In these figures, a  $\pi^0$  is simulated decaying in both the Super-Kamiokande detector and a 2km water Cherenkov detector with 8-inch and 20-inch PMTs. As can be seen, qualitatively the 8-inch case looks much more like Super-Kamiokande.

Preliminary results confirm that for reconstructing single ring muons the event selection efficiency is the same as Super-Kamiokande’s to within 1%. There is approximately a 5% difference if 20-inch PMTs are used. To finish

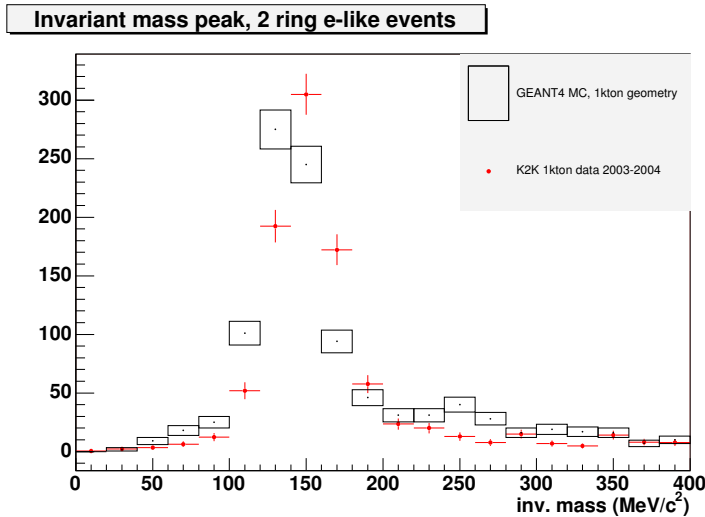


Figure 13: Comparison of the invariant mass peak for 2 ring e-like events from K2K 1kton data and GEANT4 MC configured with the geometry of the K2K water Cherenkov detector.  $\nu_\mu$  MC events were simulated using the K2K spectrum and neutrino-water interaction model.

the design of the water Cherenkov detector we must do extensive quantitative studies like the one above. Other issues we need to study are: particle identification, ring-counting, and perhaps most importantly the efficiency and purity of the reconstructed  $\nu_e$  samples.

### 7.1.2 Muon Momentum Resolution

After tuning and comparing with K2K 1kton data the GEANT4 simulator was used to simulate the geometry relevant for the T2K experiment. Mono energetic  $e^-$  and  $\mu^-$  events ranging from 30 MeV/c (150 MeV/c for  $\mu^-$ ) to 1500 MeV/c, travelling isotropically from random vertices were simulated and reconstructed using the SK/K2K software suite. In order to apply this software to a detector equipped with 8-inch PMTs, careful modifications had to be made to the reconstruction code.

As explained above, all stages of the reconstruction were checked : first the vertex (and first ring) fitter finds the position of the vertex (and the direction of the most visible ring) using timing and charge information. Then, using the vertex position information, the ring counting program determines the number of Cherenkov rings and their directions by a maximum likelihood method. Rings are classified by the PID (particle identification) program which determines whether the ring is *e-like* (a showering particle) or  *$\mu$ -like* (a non-showering particle) using another maximum likelihood method. Using this PID informa-

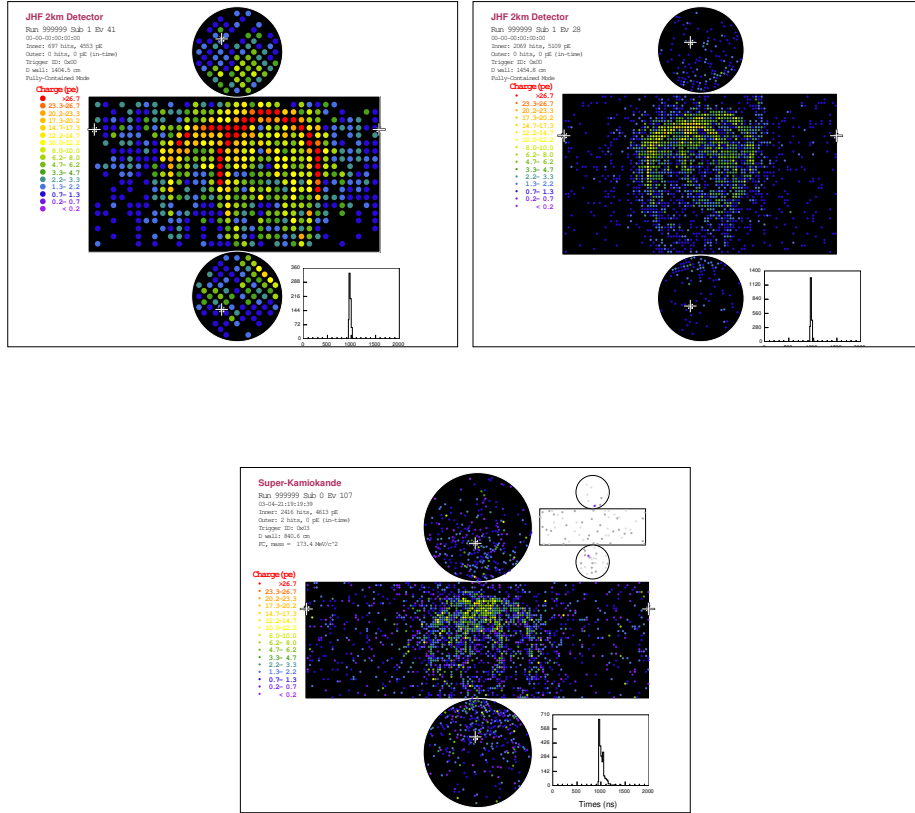


Figure 14: A simulated NC  $\pi^0$  event in the 2km WC detector with 20-inch PMTs(top left) and 8-inch PMTs (top right) Also a simulated NC  $\pi^0$  event in the Super-Kamiokande detector is shown for comparison (bottom). Based on studies with this simulation, we have concluded that it is preferable to use a larger number of small 8-inch PMTs than a smaller number of 20-inch PMTs.

tion the vertex of single-ring events is further refined. Throughout the entire process a ring separation program is used to apportion the charge of each PMT between the rings. The momentum of each track is then estimated from the amount of charge detected in a  $70^\circ$  half-opening angle around the reconstructed direction.

The performance of the vertex fitter is summarized in Figure ??, for T2K beam neutrino MC events.

Ring counting efficiency was estimated for mono-energetic single track events, and also for quasi-elastic neutrino scattering events. Figure ?? demonstrates that our detector performs similarly to SK.

PID performance will be discussed in the next section.

For the study of momentum resolution, single ring mono-energetic MC events were used. First we studied the momentum determination itself : Figure 15 shows the relation between the corrected amount of Cherenkov light and the true particle momentum. It is linear for  $e^-$ , but not  $\mu^-$  because of the non negligible muon mass. In Figure 16 the momentum resolution is also displayed, along with the best fit. In this study we estimate momentum resolution to be  $\sim \pm(0.9 + 3.6/\sqrt{P(\text{GeV})}\%$  for  $\mu^-$  and  $\sim \pm(3.0 + 1.3/\sqrt{P(\text{GeV})}\%$  for  $e^-$ .

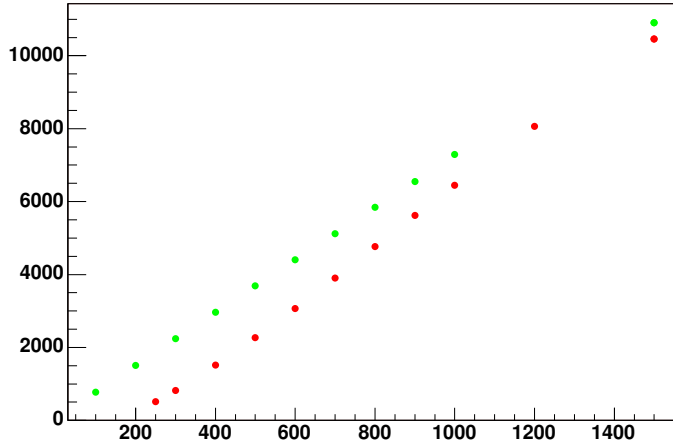


Figure 15: Relation between corrected Cherenkov light and momentum for single ring electrons and muons.

### 7.1.3 Particle Identification Performance

We can expect better particle identification (PID) performance in the 8-inch PMT case due to improved pixel resolution. In order to confirm this, a Monte Carlo study was undertaken to estimate the relative performance of the 8-inch

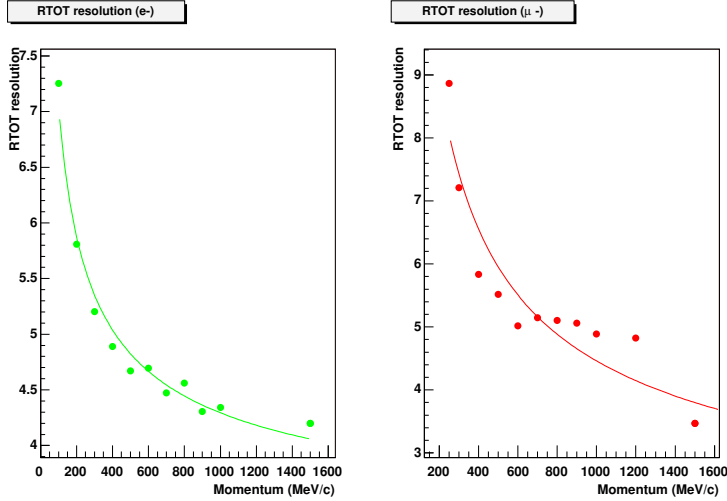


Figure 16: Momentum resolution for single ring fully-contained electrons and muons.

and 20-inch configurations. In both cases events were simulated, and then the reconstruction tool applied. For the event reconstruction, we modified the Super-K/K2K-1kton standard algorithm to match the new geometries and PMT sizes, and tuned so as to maximize the reconstruction performance, such as vertex resolution, PID, ring-counting efficiency.

Figure 17 shows the PID likelihood distribution of muons produced in the fiducial volume of the Cherenkov detector. We used charged current quasi-elastic events generated for the T2K muon neutrino beam at the 2km detector site. The distributions obtained for both the 8-inch and 20-inch PMT configurations are compared so as to reveal the shape difference of the distribution. The events for which the likelihood parameter value is less than zero are mis-identified as electrons. Clearly, the tail of the distribution has a sharper cutoff and the mis-identified events are fewer in the 8-inch case. Therefore, we conclude that better PID performance can be expected from the 8-inch configuration.

In Figure 18, the mis-identification probabilities of Super-Kamiokande and the 2km detector (8-inch case) are compared. Electrons and muons were generated within the fiducial volume with a monoenergetic spectrum, then standard event reconstruction was applied. It is important to keep PID performance at the same level as Super-Kamiokande because the acceptance of muon neutrino events is then similar, as is the reduction of the background of  $\nu_\mu \rightarrow \nu_e$  appearance measurement. Mis-identification probabilities are similar and less than about 1 % for both detectors, for all energies.

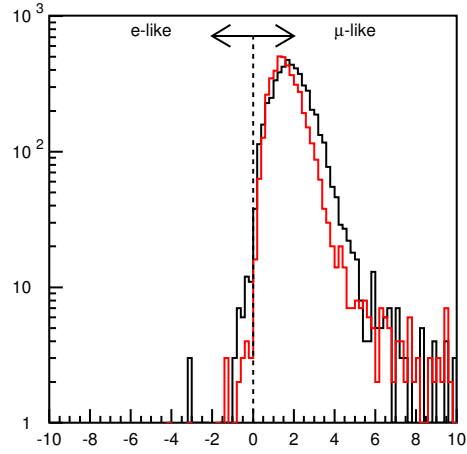


Figure 17: Likelihood parameter of particle identification estimated by muons produced in the 2km Cherenkov detector. The distribution obtained with the 8-inch PMTs configuration (red) shows the sharper tail feature and smaller mis-identification probability compared to 20-inch PMTs (black) These results support the choice of 8-inch PMTs.

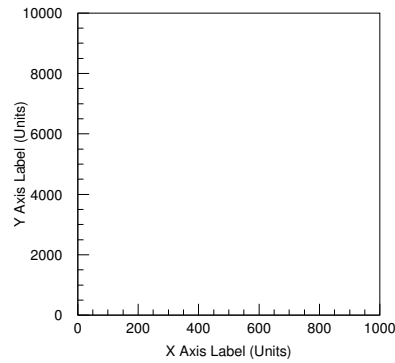


Figure 18: Mis-identified probabilities for the 2km detector (8-inch PMTs case) and Super-Kamiokande for several energy ranges.

## **7.2 Liquid Argon Simulation Results**

### **7.2.1 Muon Momentum Resolution**

### **7.2.2 Particle Identification Performance**

### **7.3 Multi-detector Reconstruction Performance**

## 8 Physics with the Intermediate Detector

*This section describes the expected physics sensitivities measurements with the 2km detector in includes results from individual detector elements plus the entire system together. This should cover the nue bg measurement and expected signal as SK as well as the measurement of the expected flux for the disappearance measurement.*

(Kearns,Casper,Mine,Walter,Rubia,Kajita,Scholberg,Fechner)

### 8.1 Measurement of the Background for $\nu_e$ Appearance

When searching for  $\nu_e$  appearance in Super-K there will be both a irreducible intrinsic  $\nu_e$  background and a background due to event misidentification. Figure 19 shows an example of the optimistic case where the a  $\nu_e$  appearance signal is found just below the current best experimental limit.

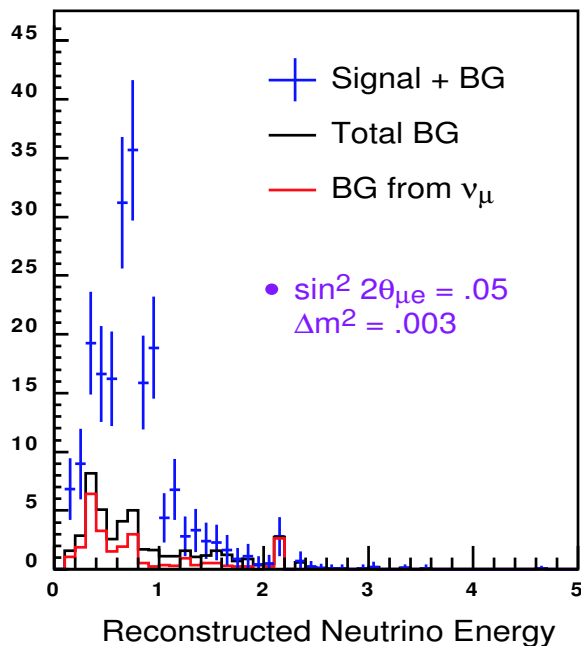


Figure 19: Expected  $\nu_e$  signal in Super-K at the current best experimental limit with a nominal background.

In this case the background is a relatively small fraction of the signal. However, if there is no observed signal, or the signal is quite small, the error or sensitivity will be dominated by how well we can determine the background to the search. Figure 20 shows this effect as a function of exposure for Super-K

with several errors on the total background normalization assumed.

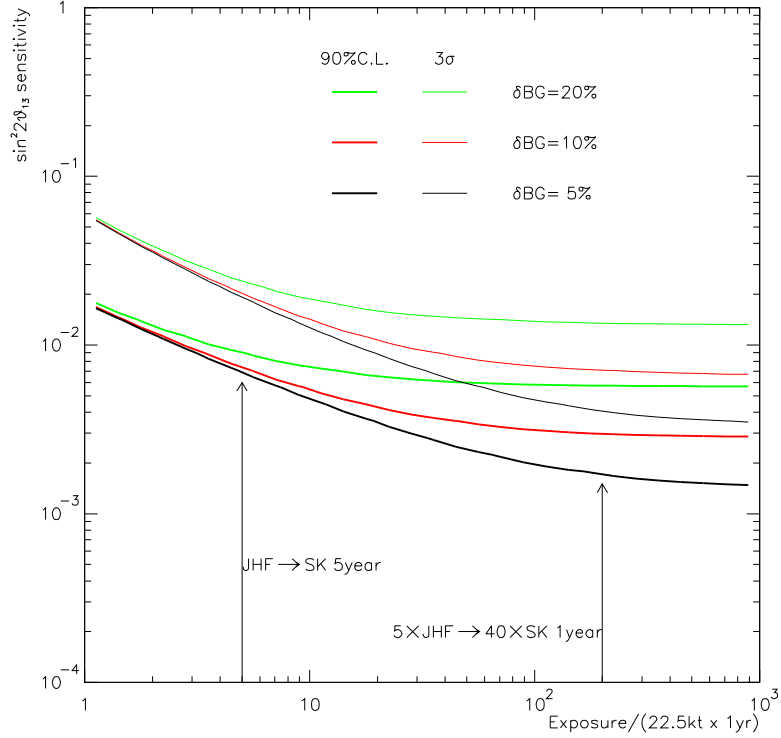


Figure 20: Sensitivity to  $\theta_{13}$  as a function of exposure for three uncertainties in the background normalization. The first arrow is the exposure for a five year T2K run, the second for five years of a upgraded JPARC beam with Hyper-Kamiokande as the target. For a five year T2K run, if the background error is more than  $\approx 10\%$  the final sensitivity will be dominated by the background error.

As can be seen, as soon as the background error becomes greater than about 10% the sensitivity at 5 years of T2K running becomes dominated by the background error. Since the other errors in reconstruction are expected to be at about the 5% level the error from far/near flux extrapolation should if at all possible be kept below 5%. This condition is clearly met by measuring the near flux at 2km.

Also shown in this figure is the error situation for a proposed second phase of T2K with an upgraded neutrino beam and approximately 20 times the fiducial volume (known as Hyper-Kamiokande). In this case the effect is even more dramatic and the total error needs to be reduced to the  $\approx 1\%$  level.

### 8.1.1 Misidentified Charged Current Background

### 8.1.2 Intrinsic Beam $\nu_e$ (from Kaons)

This proposal is concerned with the search for  $\nu_e$  appearance but the measurement of high energy (>5 GeV) muons in the 2km detector gives a important constraint on the intrinsic  $\nu_e$  background. The  $\nu_e$  signal measured in the 2km detector will be a combination of events which are really  $\nu_e$  (mostly from kaon decay), and misidentified events from  $\pi^0$  and  $\nu_\mu$  CC. As shown in Fig. 21 the highest energy neutrinos in the beam (which produce the highest energy muons) come almost exclusively from kaon decay. By measuring the high energy muon component we can independently constrain the fraction of the  $\nu_e$  background which comes from from kaon decay.

Figure 21: Breakdown of muon neutrino events at 2km from the T2K neutrino beam by parent particle type. The high energy neutrinos come predominantly from the decay of Kaons which also produce the intrinsic  $\nu_e$  background in the beam.

The uncertainty in how well we know the fraction of  $\nu_e$  in the beam from kaon decay comes from an uncertainty of how many kaons are produced in the original proton - target interaction. Especially since the detector is located off-axis, only by measuring the same beam as is seen at Super-K can we know what this fraction is to high precision.

A key part of measuring the high energy neutrino component is having a suite of detectors in the 2km complex that can work together and can be simulated together. The highest energy muons will not be contained in the water Cherenkov detector alone. Figure 22 shows the output of our MC simulation for a muon produced in the water Cherenkov detector passing through a liquid Argon TPC and into a muon ranger. Several three-dimensional views are shown in the HEPREP WIRED event display viewer, a package used by several HEP and astrophysics collaborations.

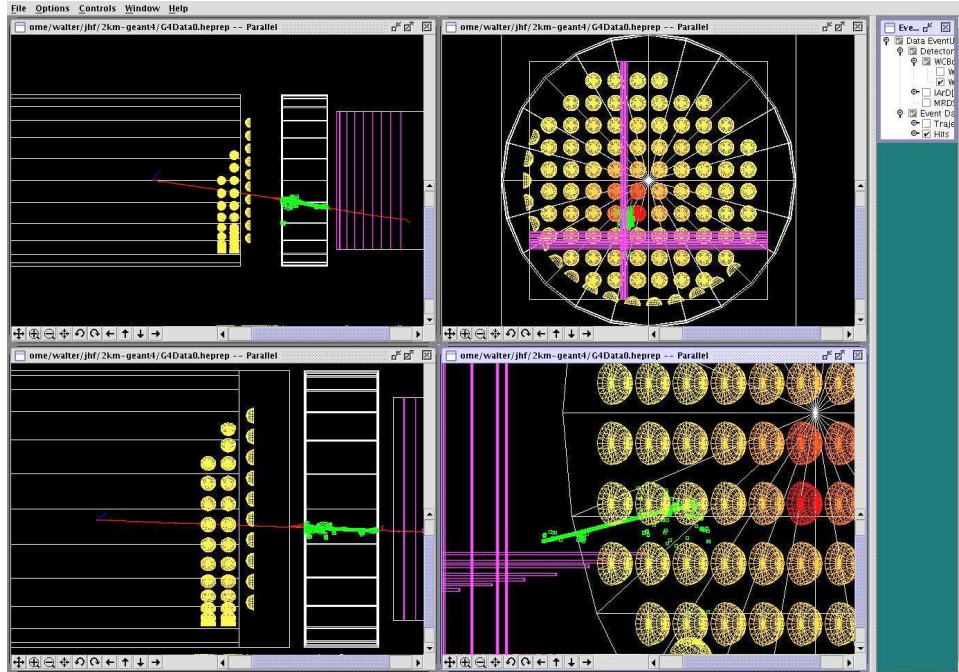


Figure 22: Multiple views of a simulated muon from a  $\nu_\mu$  CC event seen leaving the water Cherenkov detector and passing through a liquid argon TPC and into a muon ranger

### 8.1.3 Neutral Current Induced Backgrounds

#### 8.1.4 Prediction of the Background for $\nu_e$ Appearance at Super-K using the 2km detector.

## 8.2 Measurement of the Neutrino Spectrum

### 8.2.1 near/far ratio

### 8.2.2 Measurement of non-QE event rates

### 8.2.3 Expected $\theta_{23}$ and $\Delta m_{23}^2$ Sensitivity

## 8.3 Physics in the 2nd Phase T2K Experiment with the 2km Detector

As will be shown in section 8, measuring the total background to the  $\nu_e$  search is important at about the 10% level for T2K and perhaps at the 1% level for a possible next generation experiment. For this reason building a detector approximately 2km away from the neutrino production point is highly

desirable for the T2K experiment and most likely essential for a next generation experiment.

A site has already been chosen where a suitable detector can be built, and the land rights for this site negotiated with local government officials. The land will be given for the use of the T2K with no purchasing cost. The T2K beam is aimed two degrees below both Super-K and the future proposed site for the Hyper-K experiment. This is illustrated in Fig. 23.

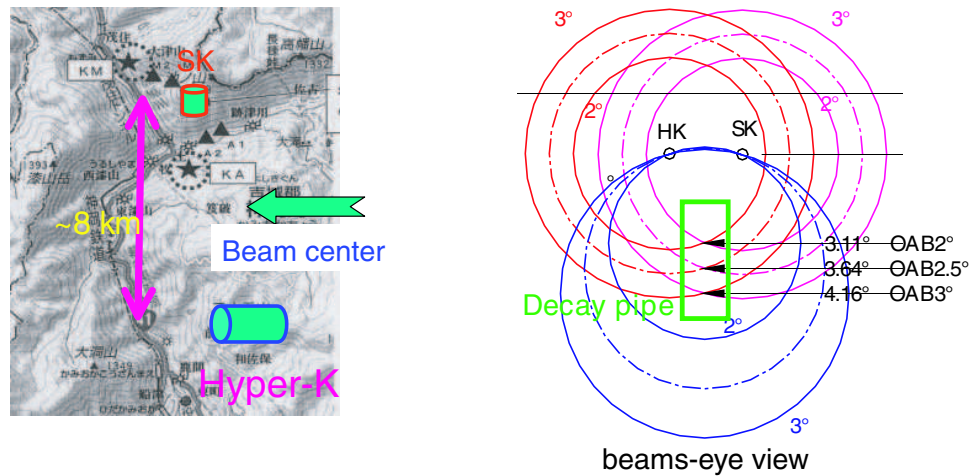


Figure 23: The position of the T2K neutrino beam relative to both Super-K and Hyper-K. The beam angle can be tuned by moving the beam up and down vertically. In this configuration both detectors are off-axis to the beam.

The proposed site for the 2km detector complex is in line with the portion of the beam that would be seen by the Hyper-K experiment. We will rely on the beam's azimuthal symmetry (as measured 280 meters away from the production point) to predict the flux and the Super-K position. The choice of this position is partly driven by cost, since hills in the line of site of SK would increase the depth of drilling of the experimental hall.

## 9 Conclusion

We gratefully acknowledge the cooperation of the Kamioka Mining and Smelting Company. The Super-Kamiokande experiment has been built and operated from funding by the Japanese Ministry of Education, Science, Sports and Culture, and the United States Department of Energy.

## References

- [1] M. Antonello et al. Detection of cherenkov light emission in liquid argon. *Nucl. Instrum. Meth.*, A516:348–363, 2004.
- [2] The Super-Kamiokande Collaboration. The super-kamiokande detector. *Nucl. Instr. Meth. A*, 501:418, 2003.

## A Schedule

## B Budget

### B.1 Water Cherenkov Detector

The detailed cost estimates for the Water Cherenkov(WC) detector are detailed below. All of these costs are based on previous are rececnt experince in builing the IMB, Kamiokande, Super-Kamiokande, and K2K 1kton tanks.

Table 1 summarizes the costs for the WC HV power supply and distribution system:

Qty	Model	Description	Unit Cost	Total cost
5	UV-1458	HV Mainframe (16 cards each)	\$12,900	\$65,000
80	UV-1461	HV Module (12 channels each)	1,935	155,000
5	-	Paddle card crate with power supply	500	17,000
5	-	Paddle cards (12 channels each)	400	264,000
Total (including spares)				US\$501,000

Table 1: Cost of PMT HV system components.

Table 2 summarizes the costs for the GPS system which synchronizes the 2km and SK sites in time:

Item	Model	Qty. req.	Unit price	Item Total	Total
Commercial equipment:					
GPS Clock	Truetime XL-DC	4	\$8,000	\$32,000	
GPS Clock	Motorola M12+	4	300	1,200	
VME crate	-	4	2,000	8,000	
VME-PC interface	Bit3	4	2,000	8,000	
Ru-stabilized oscillators	Stanford PRS-10	4	2,200	8,800	
Antennas and cabling	-	4	800	3,200	
Host/control Linux PC	-	4	1,900	7,600	
Mobilization and shipping				2100	
SUB-TOTAL					70,900
Custom LTC board					
PCB etching, drilling	-	4	23.21	93	
PCB setup and testing	-	4	459.2	1,837	
All other parts	-	4	500	2,000	
Board assembly (at UW)					
Mobilization and shipping	-	-		2000	
Board assembly labor	-	200 hr	15	3,000	
SUB-TOTAL					8,930
TOTAL					79,830

Table 2: Cost of GPS time synchronization system, to equip 2 sites, including spares.

All of the above costs are summarized in Table 3.

Item	Model	Qty. req.	Unit price	Item Total	Total
------	-------	-----------	------------	------------	-------

Table 3: Total Costs for the WC detector